Crystal Structures and Spectroscopic Characterization of Four Synthetic Cathinones: 1-(4-Chlorophenyl)-2-(Dimethylamino)Propan-1-One (N-Methyl-Clephedrone, 4-CDC), 1-(1,3-Benzodioxol-5-yl)-2-(Tert-Butylamino)Propan-1-One (tBuONE, Tertylone, MDPT), 1-(4-Fluorophenyl)-2-(Pyrrolidin-1-yl)Hexan-1-One (4F-PHP) and 2-(Ethylamino)-1-(3-Methylphenyl)Propan-1-One (3-Methyl-Ethylcathinone, 3-MEC)

Marta Siczek [1,*], **Miłosz Siczek** [2], **Paweł Szpot** [1,3], **Marcin Zawadzki** [1,3] and Olga Wachełko [2]

[1] Wroclaw Medical University, Department of Forensic Medicine, 4 J. Mikulicza-Radeckiego Street, Wroclaw 50345, Poland; pawel.szpot@umed.wroc.pl (P.S.); marcin.zawadzki@umed.wroc.pl (M.Z.)
[2] University of Wroclaw, Faculty of Chemistry, 14 Joliot-Curie, Wroclaw 50383, Poland; milosz.siczek@chem.uni.wroc.pl (M.S.); olga.wachelko@gmail.com (O.W.)
[3] Institute of Toxicology Research, 45 Kasztanowa Street, Borowa 55093, Poland
* Correspondence: marta.siczek@umed.wroc.pl; Tel.: +4871-7841-465

Abstract: Every year new synthetic cathinones are flooding the European drug market. They gain more and more popularity in place of cathinones that became illegal. Compounds from both groups, "classic" and "new" cathinones, have a similar chemical structure and, as a consequence, their psychoactive properties are not much different. Cathinone analogs were secured by the police during the search of a suspect's apartment. The aim of this paper was to present results of analyses and identification of these synthetic cathinones. The structure of new psychoactive substances (NPS) was identified by single-crystal X-ray analysis, solution nuclear magnetic resonance (NMR), UHPLC-QQQ-MS/MS and GC-MS.

Keywords: 1-(4-chlorophenyl)-2-(dimethylamino)propan-1-one; 1-(1,3-benzodioxol-5-yl)-2-(tert-butylamino)propan-1-one; 1-(4-fluorophenyl)-2-(pyrrolidin-1-yl)hexan-1-one; 2-(ethylamino)-1-(3-methylphenyl)propan-1-one; new psychoactive substances; synthetic cathinones; X-ray crystallography; solution NMR spectroscopy; mass spectrometry

1. Introduction

Recently, a new class of psychoactive substances, synthetic cathinones, has emerged on the drug-use market. Each year the European Union (EU) warning system operated by the European Monitoring Centre for Drugs and Drug Addiction (EMCDDA) notifies the appearance of new synthetic cathinone derivatives. Those compounds are the second biggest (after synthetic cannabinoids) group of new psychoactive substances monitored by the EMCDDA. According to the last report, the group of monitored synthetic cathinones consists of 130 substances. Synthetic cathinones are related to the parent cathinone, one of the psychoactive substances naturally present in khat (*Catha edulis*). Cathinone derivatives can be also considered as the β-keto analogues of amphetamine [1].

Cathinone derivatives can easily pass through the brain–blood barrier and because of structural similarities with phenethylamine, they display psychoactive properties. The most important mechanism of action of cathinones is inhibiting of protein-transporting monoamines (dopamine, noradrenaline and serotonin) of the synaptic gap. The sympathomimetic syndrome dominates in a clinical picture [2,3].

Due to the properties of synthetic cathinones, attempts have been made to use them in medicine. In the first half of the twentieth century, they were used to treat parkinsonism, depression and obesity, but because of the danger they brought, the efforts to use them for medical purposes were abandoned. Synthetic cathinones gained interest in the illegal drug market after 2000, when they began to be used as "legal highs". Since then, further cathinones were synthesized and marketed, posing a real threat to public health [4,5].

Cathinones cause a number of side effects associated with the cardiovascular system (increased heart rate, arrhythmias, increased blood pressure, myocardial ischemia with ECG changes and chest pain, myocarditis and sudden cardiac death), the coagulation system (disseminated vascular coagulation syndrome and decrease in platelet count), the nervous system (sleep disturbances, headache, vision disorder, mydriasis, paresthesia, convulsions and hyperthermia), and the gastrointestinal tract (nausea, vomiting and abdominal pain). These compounds also cause mental disorders and metabolic disorders (including metabolic acidosis, dehydration, electrolyte disorders and nitrogen body retention). The most commonly reported adverse reactions for cathinones are cardiovascular, nervous, and psychiatric disorders (including acute psychoses).

To the best of the authors' knowledge, the first synthesis of a synthetic cathinone was described in 1928 by Hyde et al. [6]. Cathinone derivatives occurring on the drug market leads to compounds that can be divided into four groups:

a) cathinones modified on C-α (alkylation is the most popular);

b) N-alkylated cathinones—one or two alkyl group attached to the nitrogen atom, it is also possible to incorporate the nitrogen atom into the pyrrolidine ring;

c) cathinones containing a modified aromatic ring, e.g., an alkyl or halogen substituent, as well as additional 3,4-methylenedioxy group that can be attached to the phenyl ring; and

d) compounds with two or more of the above-mentioned modifications [7].

The popularity of synthetic cathinones results in numerous publications devoted to their analysis using various research methods among which LC-MS remains the most popular [8–16]. Successful attempts are also being made regarding identification of specific enantiomers of synthetic cathinones by various spectroscopic methods [17,18]. X-ray diffraction methods are also widely applied for NPS analyses. Both powder diffraction and single-crystal X-ray crystallography provide valuable information on the structure of these compounds and help in their identification [14,19]. Therefore, enlarging the database of the crystal structures of synthetic cathinones can significantly facilitate the analysis of material evidence to law enforcement authorities.

Herein we report the results of the analysis of four cathinones: 4-CDC, tBuONE, 4F-PHP and 3-MEC (**1–4**, Figure 1), carried out using various instrumental methods. The analyzed samples were products seized by the police during the apartment search. To the best of the authors' knowledge, all presented crystal structures for **1–4** are published for the first time. Chromatographic analyses of Compounds **1–4** (GC-MS) and NMR data for **1–4** were reported before [20–25]. They are convergent with our results. 4F-PHP was also studied in a toxicokinetic context [26].
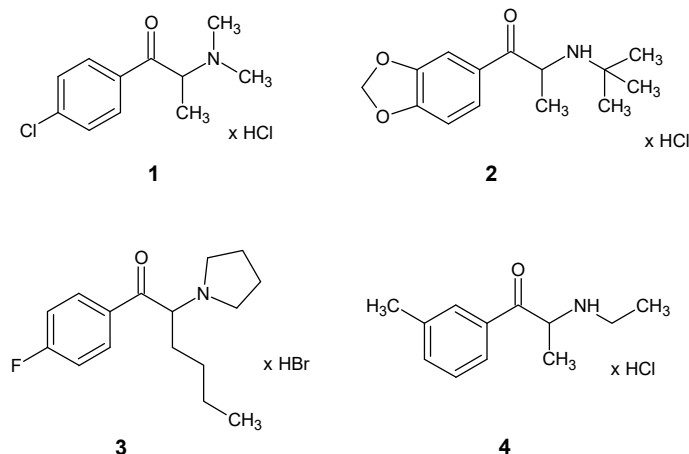
Figure 1. Structures of 1-(4-chlorophenyl)-2-(dimethylamino)propan-1-one hydrochloride (**1**), 1-(1,3-benzodioxol-5-yl)-2-(tert-butylamino)propan-1-one hydrochloride (**2**), 1-(4-fluorophenyl)-2-(pyrrolidin-1-yl)hexan-1-one hydrobromide (**3**) and 2-(ethylamino)-1-(3-methylphenyl)propan-1-one hydrochloride (**4**).

2. Materials and Methods

2.1. Chemicals

Chemicals and reagents used in analyses were acetonitrile, methanol, water (Chem Solve LC–MS, Witko, Łódź, Poland), ammonium formate (Fluka, Seelze, Germany), formic acid (Sigma-Aldrich, Darmstadt, Germany) and DMSO-d_6 (Sigma-Aldrich, Darmstadt, Germany).

2.2. Samples

Analyzed compounds have been seized by the police during the search of an apartment. Secured evidence (Figure 2) in the form of a white crystalline powder was packed in sachets of two different sizes: one of them contained 1 g, the other 0.5 g. Performed analyzes showed that each of the evidence contained only one of the psychoactive substances described in this paper.
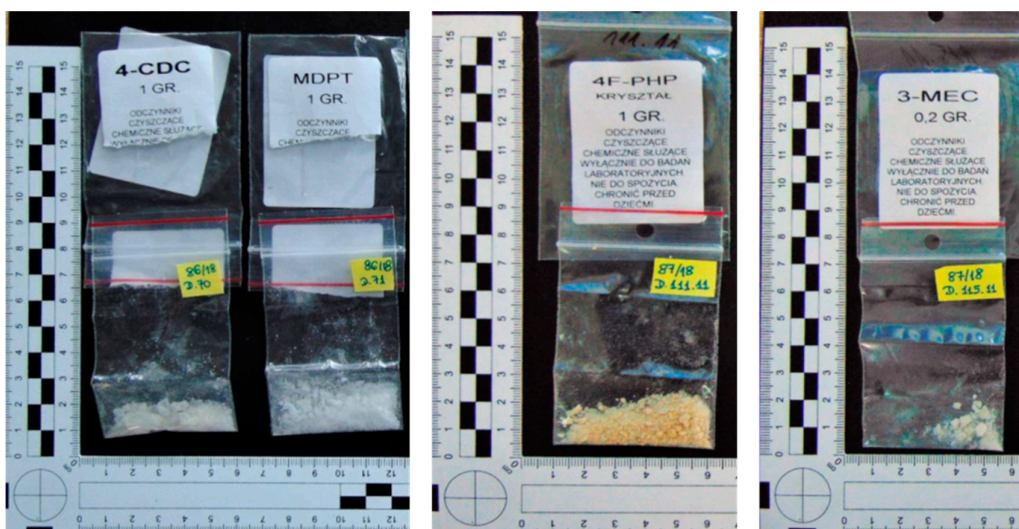

Figure 2. Material evidence seized by the police. **From left to right**: 1-(4-chlorophenyl)-2-(dimethylamino)propan-1-one hydrochloride (**1**), 1-(1,3-benzodioxol-5-yl)-2-(tert-butylamino)propan-1-one hydrochloride (**2**), 1-(4-fluorophenyl)-2-(pyrrolidin-1-yl)hexan-1-one hydrobromide (**3**) and 2-(ethylamino)-1-(3-methylphenyl)propan-1-one hydrochloride (**4**).

2.3. X-Ray Crystallography

X-ray quality crystals were taken directly from crude sample (sachet content). Single-crystal data collection was performed on a KUMA diffractometer (Rigaku Americas Holding Company, Inc. The Woodlands, Texas, TX, USA) with a Saphire CCD detector, equipped with an Oxford Cryosystems open-flow nitrogen cryostat, using ω-scan and graphite-monochromated Mo K$_\alpha$ (λ = 0.71073 Å) radiation at 100 K. Cell refinement, data reduction, analysis and absorption correction were carried out with CRYSALIS^{Pro} [27] software. The structures were solved by direct methods with SHELXS [21], and refined with full-matrix least-squares techniques on F^2 with SHELXL [28]. All hydrogen atoms were calculated in idealized geometry riding on their parent atoms. The molecular structure plots were prepared using Diamond [29]. Full details can be found in the CIF files CCDC 1945259–1945262.

2.4. NMR Spectra

NMR spectra were recorded in DMSO-d_6 at room temperature on a Bruker 500 MHz Avance II spectrometer (Billerica, Massachusetts, MA, USA) (^{1}H frequency 500.13 MHz, ^{13}C 125.7 MHz). Spectra were referenced to the residual solvent signals (2.50 and 39.5 ppm). 2D experiments (COSY, HSQC, HMBC) were performed by means of standard Bruker software, recorded with 2048 data points in the t_2 domain and up to 1024 points in the t_1 domain, with a 0.5–1 s recovery delay.

2.5. LC-MS/MS Analysis

A total of 100 mg of the sample was dissolved in 5 mL of methanol and diluted 1000-fold with MeOH. A total of 10 μL of diluted solution was transferred to a 150 μL insert containing 80 μL of MeOH and 10 μL of IS (4-MMC-d_3, c = 1μg/mL), mixed on a vortex and analyzed with UHPLC-QQQ-MS/MS.

Analyses were performed using an ultra-high-performance liquid chromatograph (Nexera X2, Shimadzu, Kyoto, Japan). The separation was done using a Kinetex XB-C18 2.6 μm 2.1 mm × 150 mm column (Phenomenex, Torrance, California, CA, USA) with the thermostat set at 40 °C. The mobile phase consisted of a mixture of 10 mM ammonium formate and 0.1% formic acid in water (A) and 0.1% formic acid in acetonitrile (B). The gradient elution was carried out at a constant flow of 0.4 mL/min. The gradient applied was as follows: 0 min, 5% B; 12 min, 98% B; 14 min, 98% B; and 15 min, 5% B. A return to the initial gradient compositions (95% A and 5% B) was performed at 5 min.

Detection of the investigated compounds was achieved using a triple-quadrupole mass spectrometer (LCMS-8050, Shimadzu, Kyoto, Japan). The spectrometer was equipped with an ESI source; determination of the investigated substances was carried out in the Scan mode with positive ionization, and mass range of 50–1000 *m/z*. The following MS parameters were fixed: nebulizing gas flow, 3 L/min; heating gas flow, 10 L/min; interface temperature, 250 °C; DL temperature, 200 °C; heat block temperature, 350 °C; and drying gas flow, 10 L/min.

2.6. GC-MS Analysis

A 100 mg sample was dissolved in 5 mL of methanol and analyzed with GC-MC. Gas chromatography–mass spectrometry (GC-MS) analyses were performed using a gas chromatograph coupled with a triple quadrupole mass spectrometer (GC-MS-TQ8040; Shimadzu, Kyoto, Japan). The injector was maintained at 250 °C. Sample injection (2 μL) was in the direct mode. Separation of sample components was conducted using the ZB-5MSi column (30 m length, 0.25 mm inner diameter and 0.25 μm film thickness; Phenomenex, Torrance, California, CA, USA). Helium was used as a carrier gas at the flow rate of 2 mL min^{-1}. The mass detector was set to positive electron ionization (EI) mode and the electron beam energy was 70 eV. The mass detector was operating in a full scan mode in the 50–650 amu range.

3. Results and Discussion

It has been shown that single-crystal X-ray analysis and solution NMR spectroscopy are methods that unambiguously identify isomers of analyzed compounds. In the context of the controlled

substances analysis, results obtained with these methods are crucial because, in the absence of an appropriate reference standard, this is not always possible using routinely used technics such as LC-MS and GC-MS.

3.1. X-Ray Crystallography

The molecular structures of 4-CDC(**1**), MDPT(**2**), 4F-PHP(**3**) and 3-MEC(**4**) are presented in Figures 3, 5, 7 and 9, while representative bond lengths and angles are given in Tables S1–S4 (Supplementary Information). Crystal data and structure refinement details for 4-CDC(**1**), MDPT(**2**), 4F-PHP(**3**) and 3-MEC(**4**) are presented in Table 1. Compounds **1**–**3** crystallize in the triclinic *P*-1 space group whereas compound **4** in the monoclinic *P*2$_1$/c space group. All distances and angles are in normal range. The C=O bond distance is in a range 1.208(9)–1.225(3) Å.

Table 1. Crystal data and structure refinement for Compounds **1**–**4**.

	4-CDC	**MDPT**	**4F-PHP**	**3-MEC**
Chemical formula	[C$_{11}$H$_{15}$ClNO]Cl	[C$_{14}$H$_{20}$NO$_3$]Cl	[C$_{16}$H$_{23}$FNO]Br	[C$_{12}$H$_{18}$NO]Cl
Formula Mass	248.14	285.76	344.26	227.72
Crystal system	triclinic	triclinic	triclinic	monoclinic
a(Å)	7.071(3)	7.290(3)	10.004(8)	7.518(3)
b(Å)	7.219(3)	8.376(3)	12.721(9)	26.055(9)
c(Å)	12.010(5)	12.686(5)	14.362(9)	6.991(3)
α(°)	74.83(3)	101.54(3)	65.14(4)	
β(°)	86.72(3)	98.01(3)	86.52(5)	113.09(4)
γ(°)	85.16(3)	97.50(3)	78.95(5)	
Unit cell volume (Å^3)	589.2(4)	741.5(5)	1627(2)	1259.7(9)
Temperature (K)	100(2)	100(2)	100(2)	100(2)
Space group	*P*-1	*P*-1	*P*-1	*P*2$_1$/c
No. of formula units per unit cell, *Z*	2	2	4	4
Radiation type	MoKα	MoKα	MoKα	MoKα
Absorption coefficient, *μ* (mm^{-1})	0.524	0.261	2.532	0.279
No. of reflections measured	6239	5035	12021	9302
No. of independent reflections	3536	3127	6019	3312
R$_{int}$	0.0349	0.0416	0.0683	0.0482
Final *R$_1$* values (*I* > 2σ(*I*))	0.0487	0.0539	0.0937	0.0524
Final *wR*(*F^2*) values (*I* > 2σ(*I*))	0.1318	0.1367	0.2386	0.1310
Final *R$_1$* values (all data)	0.0523	0.0610	0.1417	0.0657
Final *wR*(*F^2*) values (all data)	0.1389	0.1475	0.2975	0.1423

The asymmetric unit of crystal **1** consists of one cation [4-CDC]$^+$ and one chloride anion (Figure 3). The crystal structure of **1** is stabilized by N-H⋯Cl and C-H⋯Cl hydrogen bonds created between organic cations and chloride anions (listed in Table 2). As shown in Figure 4, organic cations are connected to each other a via N-H⋯Cl hydrogen bonds.
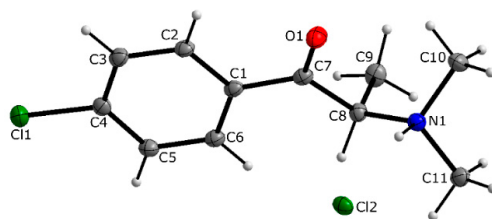

Figure 3. The molecular structure of 1-(4-chlorophenyl)-2-(dimethylamino)propan-1-one hydrochloride (**1**), showing the atom-labelling scheme.

Table 2. Hydrogen-bond geometry (Å,°) for Compound **1**.

D—H⋯*A*	*D*—H	H⋯*A*	*D*⋯*A*	*D*—H⋯*A*
N1—H1⋯Cl2	1.00	2.14	3.0386 (19)	149
C8—H8⋯Cl2^i	1.00	2.72	3.645 (2)	154

| C11—H11*C*···Cl2ii | 0.98 | 2.72 | 3.654 (2) | 160 |

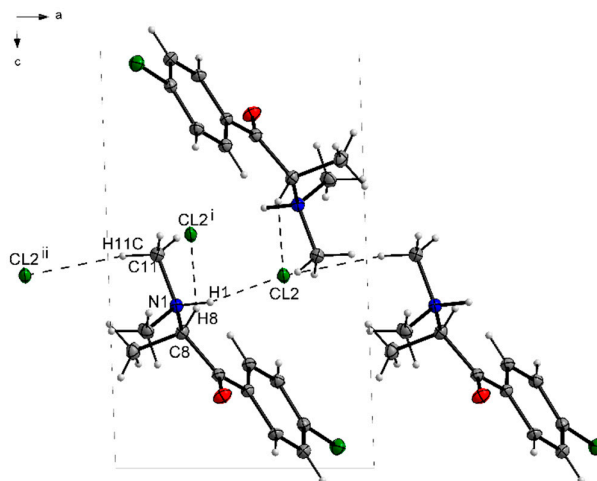Symmetry codes: (i) −*x* + 1, −*y* + 1,−*z* + 1; (ii) *x* − 1, *y*, *z*.

Figure 4. Part of the crystal structure of Compound **1** viewed along the *b* axis, showing H-bonding between neighboring ions (dashed lines). Symmetry codes: (i) − *x* + 1, −*y* + 1, −*z* + 1; (ii) *x* − 1, *y*, *z*.

The crystal structure of **2** (Figure 5) is built up from one [MDPT]⁺ cation and chloride anion: These components are held together by N–H···Cl, C–H···Cl and C–H···O hydrogen bonding (Table 3, Figure 6). More specifically, organic cations [MDPT]⁺ are hydrogen-bonded via the two Cl anions to form dimers. The crystal lattice is further supported by the weak C–H···O hydrogen bonding between the [MDPT]⁺ cations.
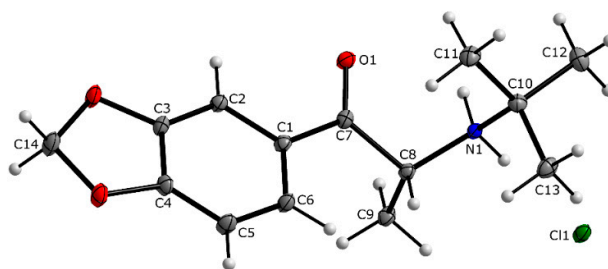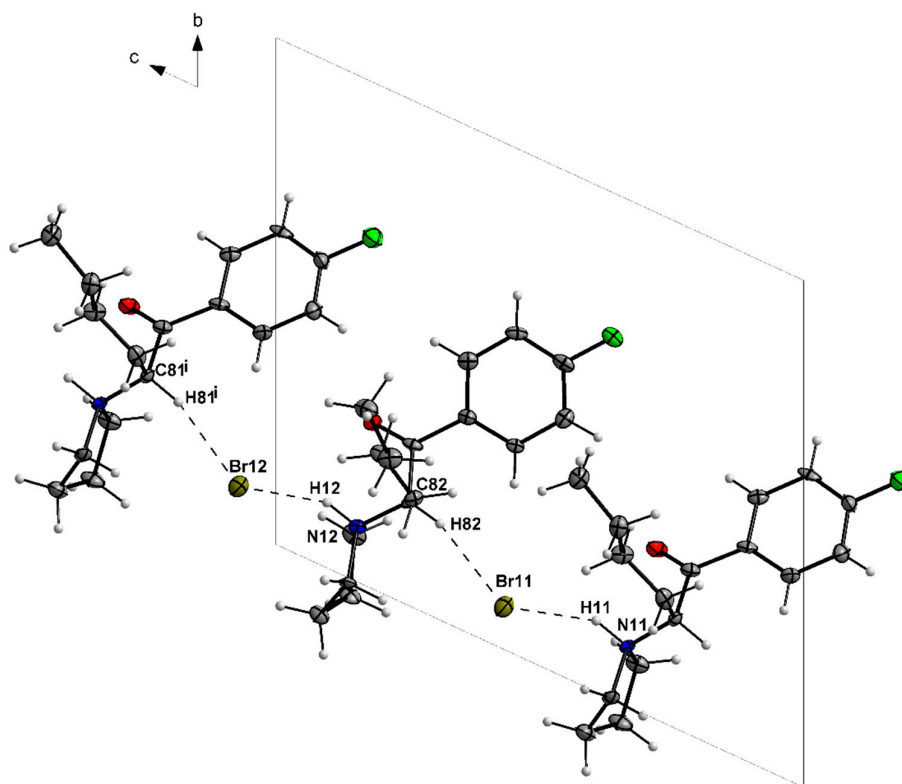

Figure 5. The molecular structure of 1-(1,3-benzodioxol-5-yl)-2-(tert-butylamino)propan-1-one hydrochloride (**2**), showing the atom-labelling scheme.

Table 3. Hydrogen-bond geometry (Å, °) for Compound **2**.

D—H···*A*	*D*—H	H···*A*	*D*···*A*	*D*—H···*A*
N1—H1*A*···Cl1i	0.91	2.36	3.178 (2)	150
N1—H1*B*···Cl1	0.91	2.24	3.149 (2)	175
C5—H5···O1ii	0.95	2.54	3.364 (3)	145
C14—H14*A*···Cl1iii	0.99	2.75	3.569 (3)	141
C8—H8···Cl1iv	1.00	2.70	3.523 (3)	140

Symmetry codes: (i) −*x* + 1, −*y* + 1,−*z* + 1; (ii) *x* − 1, *y*, *z*; (iii) *x*, *y* + 1, *z* + 1; (iv) −*x*, −*y* + 1, −*z* + 1.

Figure 6. Part of the crystal structure of Compound **2**, showing H-bonding between neighboring ions (dashed lines). Symmetry codes: (i) −*x* + 1, −*y* + 1, −*z* + 1; (ii) *x* − 1, *y*, *z*; (iii) *x*, *y* + 1, *z* + 1; (iv) −*x*, −*y* + 1, −*z* + 1.

The 4F-PHP (**3**) crystallizes with two organic cations and two bromide anions in the asymmetric unit. Examination of the two independent the 4F-PHP cations shows a subtle difference in the geometry of the *n*-butyl group. The crystal packing of Compound **3** reveals intermolecular N-H···Br, C-H···Br and C-H···F interactions between the organic cations and the Cl anions (Figures 7 and 8, Table 4).

Figure 7. The molecular structure of 1-(4-fluorophenyl)-2-(pyrrolidin-1-yl)hexan-1-one hydrobromide (**3**), showing the atom-labelling scheme.
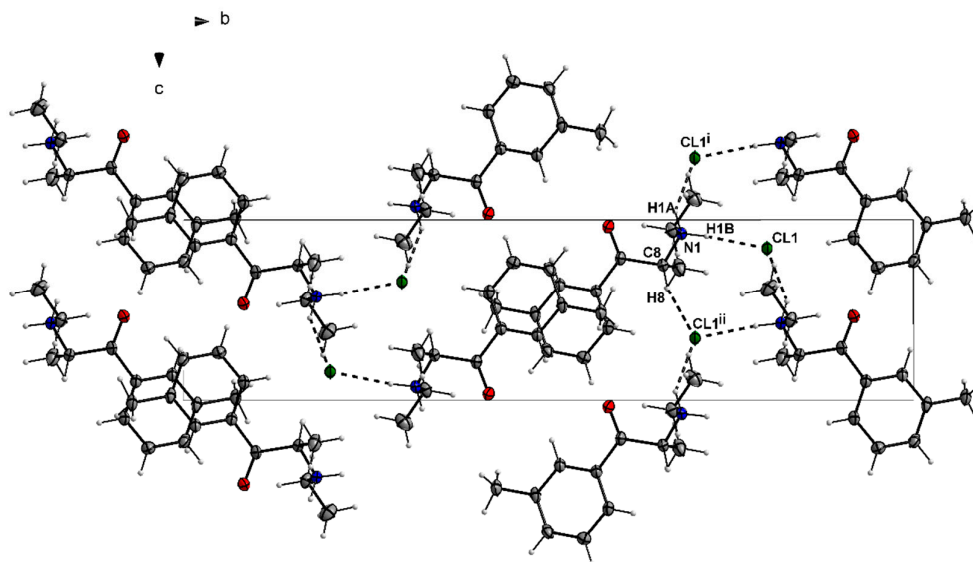
Figure 8. Part of the crystal structure of Compound **3** viewed along the *a* axis, showing H-bonding between neighboring ions (dashed lines). Symmetry code: (i) *x*, *y*, *z* − 1.

Table 4. Hydrogen-bond geometry (Å,°) for Compound **3**.

D—H···*A*	*D*—H	H···*A*	*D*···*A*	*D*—H···*A*
N11—H11···Br11	1.00	2.30	3.199 (6)	149
C81—H81···Br12[i]	1.00	2.64	3.591 (8)	159
N12—H12···Br12	1.00	2.25	3.167 (6)	152
C82—H82···Br11	1.00	2.61	3.565 (8)	160

Symmetry code: (i) *x*, *y*, *z* − 1.

The crystal of compound **4** consists of one anion [4-MEC]$^+$ and one chloride anion (Figure 9). The crystal structure is stabilized by N-H···Cl and C-H···Cl hydrogen bonds created between organic cations and chloride anions (listed in Table 5). The N-H···Cl hydrogen bond connects -NH$_2$ with Cl anion in a zigzag fashion and forms columns along the *c* axis (Figure 10).
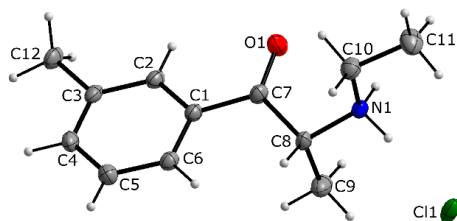
Figure 9. The molecular structure of 2-(ethylamino)-1-(3-methylphenyl)propan-1-one hydrochloride (**4**), showing the atom-labelling scheme.

Table 5. Hydrogen-bond geometry (Å,°) for Compound **4**.

D—H⋯*A*	*D*—H	H⋯*A*	*D*⋯*A*	*D*—H⋯*A*
N1—H1*A*⋯Cl1ⁱ	0.91	2.30	3.106 (2)	148
N1—H1*B*⋯Cl1	0.91	2.20	3.1067 (17)	174
C8—H8⋯Cl1ⁱⁱ	1.00	2.51	3.482 (2)	163

Symmetry codes: (i) *x*, −*y* + 3/2, *z* − 1/2; (ii) *x*, −*y* + 3/2, *z* + 1/2.

Figure 10. Part of the crystal structure of Compound **4** viewed along the *a* axis, showing H-bonding between neighboring ions (dashed lines). Symmetry codes: (i) *x*, −*y* + 3/2, *z* − 1/2; (ii) *x*, −*y* + 3/2, *z* + 1/2.

3.2. NMR Spectra

Conclusion and findings regarding the structure of analyzed compounds based on X-ray analysis results were confirmed by interpretation of solution NMR spectroscopy data. ¹H NMR spectra for all analyzed samples display one set of signals coming from the examined compound.

All signals in ¹H NMR spectra were unambiguously assigned due to 2D NMR and ¹³C NMR experiments (see Supplementary Information). Figures 11–15 show selected representative 1D and 2D NMR spectra of analyzed compounds.

Protons of substituted phenyl rings give signals in a range characteristic for aromatic systems (7.1–8.3 ppm). Signals derived from substituents on the phenyl ring appeared in the spectra of Compounds **2** (methylene at 6.20 ppm) and **4** (methyl at 2.41 ppm). The proton attached to C_α can be observed at 5.40 (4-CDC), 5.19 (MDPT), 5.52 (4F-PHP) and 5.19 (3-MEC). Broad peaks with the highest chemical shifts can be assigned to the N-H protons of analyzed compounds. In case of **1** and **3**, only one signal is observed (10.45 ppm and 10.21 ppm, respectively). For MDPT and 3-MEC two diastereotopic protons attached to the nitrogen atom yielded double broad singlets (δ = 9.38 and 8.47 for **2**; δ = 9.30 and 8.95 for **4,** Figures 11 and 12). Peaks attributed to the methyl group attached to C_α can be observed at 1.49 ppm (Compounds **1** and **2**) and 1.45 ppm (**4**). The *n*-butyl side chain of 4F-PHP forms multiplets in the range of 2.14–0.74 ppm.
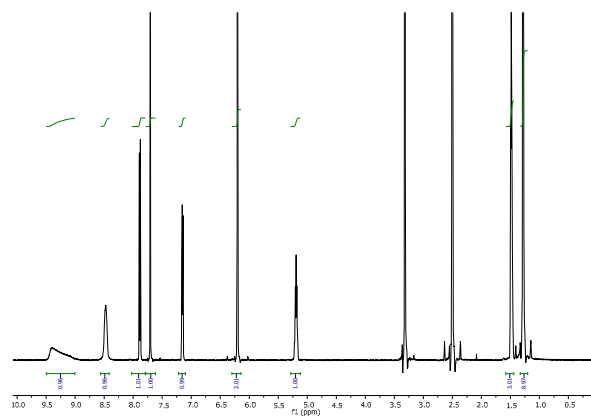
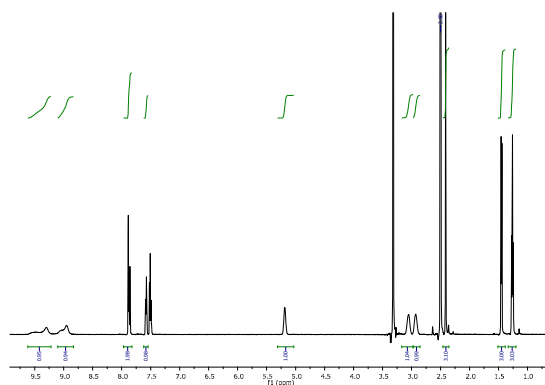**Figure 11.** ^{1}H NMR spectrum of M DPT (**2**); 500MHz, DMSO-d₆, RT.

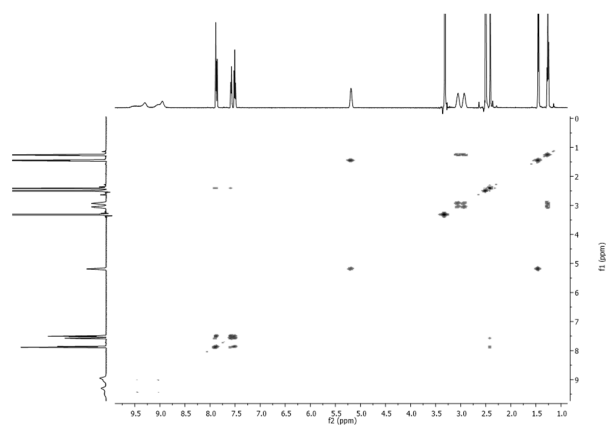**Figure 12.** ^{1}H NMR spectrum of 3-MEC (**4**); 500MHz, DMSO-d₆, RT.

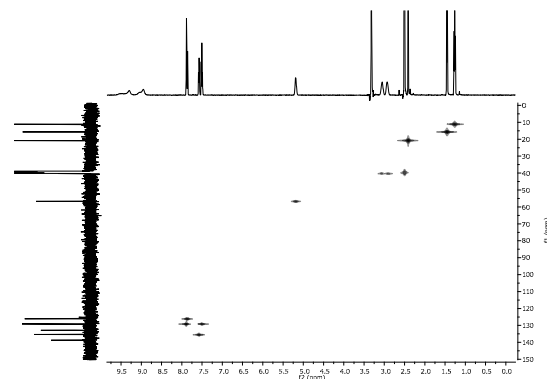**Figure 13.** COSY spectrum of 3-MEC (**4**); 500MHz, DMSO-d₆, RT.

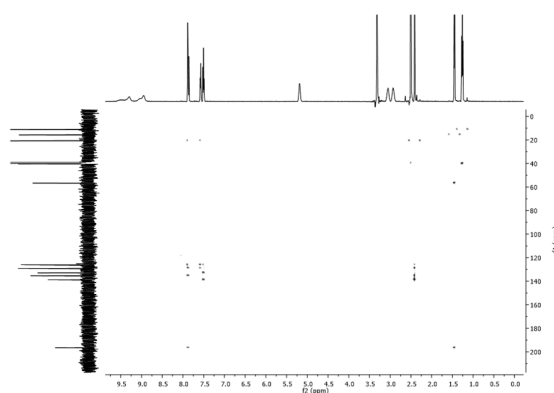**Figure 14.** ^{1}H-^{13}C HMQC spectrum of 3-MEC (**4**); 500MHz, DMSO-d$_6$, RT.

Figure 15. ^{1}H–^{13}C HMBC spectrum of 3-MEC (**4**); 500MHz, DMSO-d$_6$, RT.

Each of the described compounds is characterized by different substituents on the nitrogen atom, which is also evident in the NMR spectra. In case of 4-CDC, one singlet attributed to two methyl groups can be observed at 2.85 ppm, whereas the signal from the *tert*-butyl substituent of MDPT is located at 1.28 ppm. The 3-MEC ethyl group gives a multiplet at 1.26 ppm (three protons attached to the terminal C atom) and two broad singlets (3.05 ppm and 2.93 ppm) can be assigned to diastereotopic methylene protons. Eight protons of the pyrrolidine ring (4F-PHP) correspond to signals at 3.61, 3.48, 3.23 and 3.05 (position 2 of the pyrrolidine ring) and a multiplet at 1.96 ppm (position 3 of pyrrolidine ring).

All resonances for analyzed compounds are listed below:

4-CDC

^{1}H NMR (500 MHz, DMSO) δ: 10.45 (bs, 1H, N$^+$H), 8.08–8.03 (m, 2H, ArH *orto*), 7.78–7.63 (m, 2H, ArH *meta*), 5.40 (q, J = 7.2 Hz, 1H, C$_\alpha$H), 2.85 (s, 6H, N(CH$_3$)$_2$), 1.49 (d, J = 7.2 Hz, 3H, C$_\alpha$H$_3$).

^{13}C NMR (126 MHz, DMSO) δ: 195.3 (C=O), 139.8 (Ar-*para*), 132.1 (Ar-C$_{ipso}$), 130.8 (Ar-*orto*), 129.4 (Ar-*meta*), 64.0 (C$_\alpha$), 42.0 (N(CH$_3$)$_2$), 13.5 (CH$_3$)

MDPT

^{1}H NMR (500 MHz, DMSO) δ: 9.38 (bs, 1H, N$^+$H$_2$), 8.47 (bs, 1H, N$^+$H$_2$), 7.89 (dd, J = 8.3, 1.7 Hz, 1H, ArH-6), 7.71 (d, J = 1.7 Hz, 1H, ArH-4), 7.15 (d, J = 8.2 Hz, 1H, ArH-7), 6.20 (s, 2H, -O-CH$_2$-O-), 5.23–5.15 (m, 1H, C$_\alpha$H), 1.49 (d, J = 5.8 Hz, 3H, C$_\alpha$CH$_3$), 1.28 (s, 9H, C(CH$_3$)$_3$).

^{13}C NMR (126 MHz, DMSO) δ: 194.4 (C=O), 153.1, (Ar-C$_1$) 148.4 (Ar-C$_3$), 126.6 (Ar-C$_{ipso}$), 126.2 Ar-C$_6$), 108.7 (Ar-C$_7$), 108.2 (Ar-C$_4$), 102.6 (O-CH$_2$-O), 57.9 (**C**(CH$_3$)$_3$), 52.4 (C$_\alpha$), 25.9 (C(**CH**$_3$)$_3$), 18.5 (CH$_3$)

4F-PHP

^{1}H NMR (500 MHz, DMSO) δ 10.21 (bs, 1H, N$^+$H), 8.21–8.15 (m, 2H, ArH, *orto*), 7.49 (t, J = 8.2 Hz, 2H, ArH, *meta*), 5.52 (bs, 1H, C$_\alpha$H), 3.67–3.56 (m, 1H, PRL-1), 3.54–3.43 (m, 1H, PRL-1), 3.23 (bs, 1H, PRL-1), 3.05 (bs, 1H, PRL-1), 2.14–2.02 (m, 1H, -CH$_2$-CH$_2$-CH$_2$-), 2.02–1.85 (m, 4H, PRL-2, 1H, -CH$_2$-

CH$_2$-CH$_2$-), 1.27–1.11 (m, 3H, -CH$_2$-CH$_2$-CH$_2$-), 1.05–0.91 (m, 1H, -CH$_2$-CH$_2$-CH$_2$-), 0.74 (t, J = 6.8 Hz, 3H, CH$_3$).

^{13}C NMR (126 MHz, DMSO) δ: 195.2 (C=O), 166.5 (Ar-*para*), 132.2 (Ar-*orto*), 132.1 (Ar-C$_{ipso}$), 116.5 (Ar-*meta*), 67.7 (C$_α$), 54.0 (PRL-C$_2$), 51.9 (PRL-C$_2$), 29.3 (PRL-C$_3$), 25.5 (-CH$_2$-), 22.8 (-CH$_2$-), 21.8 (-CH$_2$-), 13.4 (-CH$_3$)

3-MEC

^{1}H NMR (500 MHz, DMSO) δ 9.30 (bs, 1H, N$^+$H$_2$), 8.95 (bs, 1H, N$^+$H$_2$), 7.91–7.84 (m, 2H, ArH-2,4), 7.61–7.55 (m, 1H, ArH-6), 7.53–7.47 (m, 1H, ArH-5), 5.19 (bs, 1H, C$_α$H), 3.05 (bs, 1H, N-CH$_2$-C), 2.93 (bs, 1H, N-CH$_2$-C), 2.41 (s, 3H, ArCH$_3$), 1.45 (d, J = 7.1 Hz , 3H, C$_α$CH$_3$), 1.26 (t, J = 7.2 Hz, 3H, CH$_2$CH$_3$).

^{13}C NMR (126 MHz, DMSO) δ: 196.5 (C=O), 138.8 (Ar-C$_{ipso}$), 135.4 (Ar-C$_6$), 132.9 (Ar-C$_3$), 129.1 (Ar-C$_2$, Ar-C$_5$), 126.1 (Ar-C$_4$), 56.7 (C$_α$), 40.3 (-CH$_2$-), 20.8 (Ar-CH$_3$), 15.7 (C$_α$-CH$_3$)11.2 (-CH$_2$-**CH$_3$**)

3.3. LC-MS/MS Analysis

4-CDC

A chromatogram in positive ion mode was dominated by ion 212.10. This, it was concluded, was a precursor ion [M+H]$^+$ of 4-CDC chosen for further Product Ion Scan mode. Retention times of 4-CDC and IS were 4.05 and 3.68 min., respectively.

MDPT

A chromatogram in positive ion mode was dominated by ion 250.10. This, it was concluded, was a precursor ion [M+H]$^+$ of MDPT chosen for further Product Ion Scan mode. Retention times of MDPT and IS were 4.22 and 3.68 min., respectively.

4F-PHP

A chromatogram in positive ion mode was dominated by ion 264.10. This, it was concluded, was a precursor ion [M+H]$^+$ of 4F-PHP chosen for further Product Ion Scan mode. Retention times of 4-CDC and IS were 5.39 and 3.68 min., respectively (Figure 16; for the rest of the MS spectra see the Supporting Information).
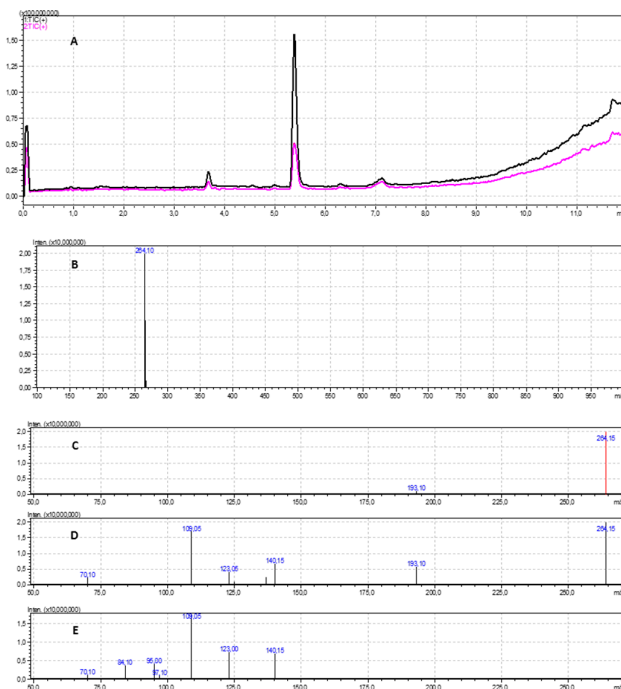

Figure 16. Total ion chromatogram (TIC) of the sample with 4F-PHP (**3**) and IS (**A**); mass spectrum of the precursor ion (**B**) and the Product Ion Scan with collision energy: −10 V, −20 V and −35 V, respectively (**C–E**).

3-MEC

A chromatogram in positive ion mode was dominated by ion 192.10. This, it was concluded, was a precursor ion [M+H]$^+$ of 3-MEC chosen for further Product Ion Scan mode. Retention times of 3-MEC and IS were 4.00 and 3.68 min., respectively.

3.4. GC-MS Analysis

GC-MS spectra for **1–4** obtained in our laboratory contained all the peaks reported in the "European project response to challenges to forensic drugs analyses" [13–16] and confirm our conclusions based on measurements carried out using other instrumental methods (Figure 17; for the rest of the GC-MS spectra see the Supporting Information).
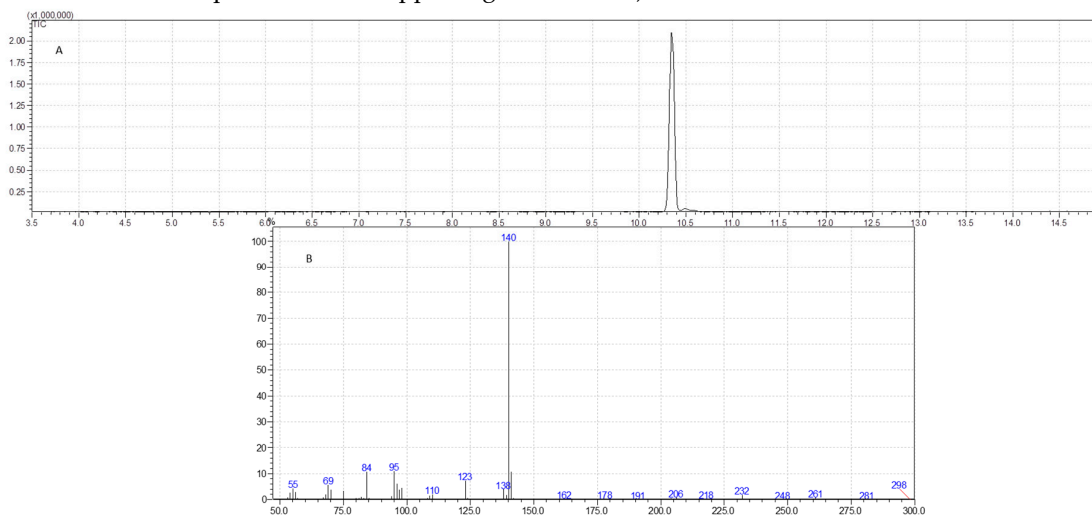

Figure 17. Gas chromatography (**A**) and mass spectrometry data (**B**) of 4F-PHP (**3**).

4. Conclusions

We presented complete chemical identification of four synthetic cathinones seized by the police from an illegal drug market in Poland. Analyzed compounds were characterized with the use of X-ray crystallography, NMR spectroscopy and mass spectrometry. X-ray data for Compounds **1–4** were presented for the first time. In view of the continuous increase in the number of compounds entering the illegal drug market, this is valuable information. It can be relevant not only to the police, but also to customs services and forensic laboratories in which such substances are analyzed and identified. Expanding the existing crystallographic database for new psychoactive substances is important because it can be successfully used in interception of illegal substances on the market and for pursuing drug synthesis prohibition.

Supplementary Materials: The following are available online at www.mdpi.com/xxx/s1, Table S1: Geometric parameters of compound 1 (4-CDC) [Å, °]; Table S2: Geometric parameters of compound 2 (MDPT) [Å, °]; Table S3: Geometric parameters of compound 3 (4F-PHP) [Å, °]; Table S4: Geometric parameters of compound 4 (3-MEC) [Å, °]; Figure S1: 1H NMR spectrum of 4-CDC (1); 500 MHz, DMSO-d6, RT; Figure S2: 13C NMR spectrum of 4-CDC (1); 126 MHz, DMSO-d6, RT; Figure S3: COSY spectrum of 4-CDC (1); 500MHz, DMSO-d6, RT; Figure S4: 1H-13C HMQC spectrum of 4-CDC (1); 500 MHz, DMSO-d6, RT; Figure S5: 1H-13C HMBC spectrum of 4-CDC (1); 500 MHz, DMSO-d6, RT; Figure S6: 13C NMR spectrum of MDPT (2); 126 MHz, DMSO-d6, RT; Figure S7: COSY spectrum of MDPT (2); 500 MHz, DMSO-d6, RT; Figure S8: 1H-13C HMQC spectrum of MDPT (2); 500MHz, DMSO-d6, RT; Figure S9: 1H-13C HMBC spectrum of MDPT (2); 500 MHz, DMSO-d6, RT; Figure S10: 1H NMR spectrum of 4F-PHP (3); 500 MHz, DMSO-d6, RT; Figure S11: 13C NMR spectrum of 4F-PHP (3); 126 MHz, DMSO-d6, RT; Figure S12: COSY spectrum of 4F-PHP (3); 500 MHz, DMSO-d6, RT; Figure S13: 1H-13C HMQC spectrum of 4F-PHP (3); 500 MHz, DMSO-d6, RT; Figure S14: 1H-13C HMBC spectrum of 4F-PHP (3); 500 MHz, DMSO-d6, RT; Figure S15: 13C NMR spectrum of 3-MEC (4); 126 MHz, DMSO-d6, RT; Figure S16: Total ion chromatogram (TIC) of sample with 4-CDC and IS (A); Mass spectrum of precursor ion (B) and Product

Ion Scan with collision energy: −10 V, −20V and −35 V respectively (C,D,E); Figure S17: Total ion chromatogram (TIC) of sample with MDPT and IS (A); Mass spectrum of precursor ion (B) and Product Ion Scan with collision energy: −10 V, −20V and −35 V respectively (C,D,E); Figure S18: Total ion chromatogram (TIC) of sample with 3-MEC and IS (A); Mass spectrum of precursor ion (B) and Product Ion Scan with collision energy: −10 V, −20V and −35 V respectively (C,D,E); Figure S19: Gas chromatography (A) and mass spectrometry data (B) of 4-CDC (1); Figure S20: Gas chromatography (A) and mass spectrometry data (B) of MDPT (2); Figure S21: Gas chromatography (A) and mass spectrometry data (B) of 3-MEC(4).

References

1. EMCDDA. European Drug Report 2018: Trends and Developments. 2018. Available online: http://www.emcdda.europa.eu/system/files/publications/8585/20181816_TDAT18001ENN_PDF.pdf (accessed on 23 April 2019).

2. Feyissa, A.M.; Kelly, J.P. A review of the neuropharmacological properties of khat. *Prog. Neuro Psychopharmacol. Boil. Psychiatry* **2008**, *32*, 1147–1166, doi:10.1016/j.pnpbp.2007.12.033.

3. Simmler, L.D.; Buser, T.A.; Donzelli, M.; Schramm, Y.; Dieu, L.H.; Huwyler, J.; Chaboz, S.; Hoener, M.C.; Liechti, M.E. Pharmacological characterization of designer cathinones in vitro. *Br. J. Pharmacol.* **2013**, *168*, 458–470, doi:10.1111/j.1476-5381.2012.02145.x.

4. Kelly, J.P. Cathinone derivatives: A review of their chemistry, pharmacology and toxicology. *Drug Test. Anal.* **2011**, *3*, 439–453, doi:10.1002/dta.313.

5. Majchrzak, M.; Celiński, R.; Kuś, P.; Kowalska Sajewicz, M. The newest cathinone derivatives as designer drugs: An analyticalband toxicological review. *Forensic Toxicol.* **2011**, *36*, 33–50, doi:10.1007/s11419-017-0385-6.

6. Hyde, J.F.; Browning, E.; Adams, R. Synthetic Homologs of d,l-ephedrine. *J. Am. Chem. Soc.* **1928**, *50*, 2287–2292, doi:10.1021/ja01395a032.

7. Valente, M.J.; Guedes de Pinho, P.; de Lourdes Bastos, M.; Carvalho, F.; Carvalho, M. Khat and synthetic cathinones: A review. *Arch. Toxicol.* **2014**, *88*, 15–45, doi:10.1007/s00204-013-1163-9.

8. Trzybiński, D.; Niedziałkowski, P.; Ossowski, T.; Trynda, A.; Sikorski, A. Single-crystal X-ray diffraction analysis of designer drugs: Hydrochlorides of metaphedrone and pentedrone. *Forensic Sci. Int.* **2013**, *232*, 28–32, doi:10.1016/j.forsciint.2013.07.012.

9. Kuś, P.; Kusz, J.; Książek, M.; Pieprzyca, E.; Rojkiewicz, M. Spectroscopic characterization and crystal structures of two cathinone derivatives: N-ethyl-2-amino-1-phenylpropan-1-one (ethcathinone) hydrochloride and N-ethyl-2-amino-1-(4-chlorophenyl)propan-1-one (4-CEC) hydrochloride. *Forensic Toxicol.* **2017**, *35*, 114–124, doi:10.1007/s11419-016-0345-6.

10. Camilleri, A.; Johnston, M.R.; Brennan, M.; Davis, S.; Caldicott, D.G. Chemical analysis of four capsules containing the controlled substance analogues 4-methylmethcathinone, 2-fluoromethamphetamine, α-phthalimidopropiophenone and N-ethylcathinone. Forensic *Sci. Int.* **2010**, *197*, 59–66, doi:10.1016/j.forsciint.2009.12.048.

11. Kolanoś, R.; Solis, E.; Sakloth, F.; De Felice, L.J.; Glennon, R.A. "Deconstruction" of the Abused Synthetic Cathinone Methylenedioxypyrovalerone (MDPV) and an Examination of Effects at the Human Dopamine Transporter. *ACS Chem. Neurosci.* **2013**, *4*, 1524–1529, doi:10.1021/cn4001236.

12. Matsuta, S.; Katagi, M.; Nishioka, H.; Kamata, H.; Sasaki, K.; Shima, N.; Kamata, T.; Miki, A.; Tatsuno, M.; Zaitsu, K.; et al. Structural characterization of cathinone-type designer drugs by EI mass spectrometry. *Jpn. J. Forensic Sci. Technol.* **2014**, *19*, 77–89, doi:10.3408/jafst.19.77.

13. Mikołajczyk, A.; Adamowicz, P.; Tokarczyk, B.; Sekuła, K.; Gieroń, J.; Wrzesień, W.; Stanaszek, R. Determination of N-ethylhexedrone, a new cathinone derivative, in blood collected from drivers—Analysis of three cases. *Probl. Forensic Sci.* **2017**, *109*, 53–63.

14. Kuś, P.; Rojkiewicz, M.; Kusz, J.; Książek, M.; Sochanik, A. Spectroscopic characterization and crystal structures of four hydrochloride cathinones: N-ethyl-2-amino-1-phenylhexan-1-one (hexen, NEH), N-methyl-2-amino-1-(4-methylphenyl)-3-methoxypropan-1-one (mexedrone), N-ethyl-2-amino-1-(3,4-methylenedioxyphenyl)pentan-1-one (ephylone) and N-butyl-2-amino-1-(4-chlorophenyl)propan-1-one (4-chlorobutylcathinone). *Forensic Toxicol.* **2019**, *37*, 456–464, doi:10.1007/s11419-019-00477-y.

15. Pauk, V.; Lemr, K. Forensic applications of supercritical fluid chromatography – Mass spectrometry. *J. Chromatogr. B* **2018**, *1086*, 184–196, doi:10.1016/j.jchromb.2018.04.015.

16. Schwaningera, A.E.; Meyerb, M.R.; Maurer, H.H. Chiral drug analysis using mass spectrometric detection relevant to research and practice in clinical and forensic toxicology. *J. Chromatogr. A* **2012**, *1269*, 122–135, doi:10.1016/j.chroma.2012.07.045.

17. Spálovská, D.; Maříková, T.; Kohout, M.; Králík, F.; Kuchař, M.; Setnička, V. Methylone and pentylone: Structural analysis of new psychoactive substances. *Forensic Toxicol.* **2019**, *37*, 366–377, doi:10.1007/s11419-019-00468-z.

18. Silva, B.; Pereira, J.A.; Cravo, S.; Araújo, A.M.; Fernandes, C.; Pinto, M.M.; de Pinho, P.G.; Remião, F. Multi-milligram resolution and determination of absolute configuration of pentedrone and methylone enantiomers. *J. Chromatogr. B* **2018**, *1100*, 158–164, doi:10.1016/j.jchromb.2018.10.002.

19. Jurásek, B.; Bartůněk, V.; Huber, S.; Kuchař, M. X-ray powder diffraction—A non-destructive and versatile approach for the identification of new psychoactive substances. *Talanta* **2019**, *195*, 414–418, doi:10.1016/j.talanta.2018.11.063.

20. European Project Response to Challenges to Forensic Drugs Analyses. Analytical Report: 4-CDC. 2016. https://www.policija.si/apps/nfl_response_web/0_Analytical_Reports_final/4-CDC-ID-1908-18_report.pdf (accessed on 1 August 2019).

21. European Project Response to Challenges to Forensic Drugs Analyses. Analytical Report: tBuONE. 2016. https://www.policija.si/apps/nfl_response_web/0_Analytical_Reports_final/tBuONE-ID-1378-15-report_final1.pdf (accessed on 1 August 2019).

22. European Project Response to Challenges to Forensic Drugs Analyses.Analytical Report: 4F-PHP. 2016. https://www.policija.si/apps/nfl_response_web/0_Analytical_Reports_final/4F-PHP-ID-1302-15rpt081216.pdf (accessed on 1 August 2019).

23. European Project Response to Challenges to Forensic Drugs Analyses. Analytical Report: 3-MEC. 2016. https://www.policija.si/apps/nfl_response_web/0_Analytical_Reports_final/3-MEC-ID-1724-16_report.pdf (accessed on 1 August 2019).

24. Maas, A.; Sydow, K.; Madea, B.; Hess, C. Separation of ortho, meta and para isomers of methylmethcathinone (MMC) and methylethcathinone (MEC) using LC-ESI-MS/MS: Application to forensic serum samples. *J. Chromatogr. B* **2017**, *1051*, 118–125, doi:10.1016/j.jchromb.2017.01.046.

25. Apirakkan, O.; Frinculescu, A.; Shine, T.; Parkin, M.C.; Cilibrizzi, A.; Frascione, N.; Abbate, V. Analytical characterization of three cathinone derivatives,4-MPD, 4F–PHP and bk-EPDP, purchased as bulk powderfrom online vendors. *Drug Test. Anal.* **2018**, *10*, 372–378, doi:10.1002/dta.2218.

26. Wagmann, L.; Manier, S.K.; Eckstein, N.; Maurer, H.H.; Meyer, M.R. Toxicokinetic studies of the four new psychoactive substances 4-chloroethcathinone, N-ethylnorpentylone, N-ethylhexedrone, and 4-fluoro-alpha-pyrrolidinohexiophenone. *Forensic Toxicol.* **2019**, 1–11, doi:10.1007/s11419-019-00487-w.

27. *CrysAlisPro*; Agilent Technologies Inc: Yarnton, Oxfordshire, UK.

28. Sheldrick, G.M. Crystal structure refinement with SHELXL. *Acta Crystallogr. Sect. C Struct. Chem.* **2015**, *71*, 3–8, doi:10.1107/S2053229614024218.

29. Brandenburg, K. *Diamond*, Version 4.0; Crystal, Molecular Structure Visualization; Crystal Impact—K. Brandenburg & H. Putz Gbr: Bonn, Germany, 2009.